Inelastic excitation and neutron transfer in the ^{13}C-^{13}C scattering with the molecular particle-core model

Artur Thiel and Walter Greiner
Institut für Theoretische Physik der Johann-Wolfgang-Goethe-Universität, Frankfurt am Main, Federal Republic of Germany

Jae Y. Park
Department of Physics, North Carolina State University, Raleigh, North Carolina 27695

Werner Scheid
Institut für Theoretische Physik der Justus-Liebig-Universität, Giessen, Federal Republic of Germany
(Received 8 December 1986)

The molecular particle-core model is applied to the scattering of ^{13}C on ^{13}C. The model divides the $^{13}C+^{13}C$ system into two ^{12}C cores and two valence neutrons. The valence neutrons are described with molecular eigenfunctions of the symmetric two-center shell model. Coupled channel calculations are carried out for the inelastic single and mutual excitation of the first $\frac{1}{2}^+$ state of ^{13}C and the neutron transfer to the $^{12}C+^{14}C$ system. The results reproduce the experimental data. The analysis of the S matrix shows that the gross structure of the transfer excitation function is related to resonances in the relative motion of the elastic and transfer channels.

I. INTRODUCTION

Since the discovery of collective nuclear molecules more than 26 years ago by Bromley, Kuehner, and Almqvist,[1] there has also been experimental and theoretical work on the problem of the molecular single-particle motion in the collision of two light heavy ions. For a recent review of the field see the article of Imanishi and von Oertzen.[2]

Two approaches can be used to describe the formation of molecular orbitals in light nucleus-nucleus collisions. The first one, the molecular particle-core model, takes up the close relationship of the molecular idea to the concept of the two-center shell model[3,4] (TCSM) and treats the motion of the outermost bound nucleons in terms of single-particle states of the TCSM with a potential generated by all nucleons. This model has been introduced by Park *et al.*[5] and studied by Park *et al.*,[6] Terlecki *et al.*,[7] and Könnecke *et al.*[8] In the second approach the molecular orbitals of the nucleons are described by the method of linear combinations of nuclear orbitals (LCNO). This method and the corresponding reaction theory have been originally developed by von Oertzen and Nörenberg,[9] and by Becker *et al.*[10] and applied, e.g., by Imanishi and von Oertzen[2] to the system $^{12}C + ^{13}C$.

A very interesting system with respect to molecular orbitals is the $^{13}C + ^{13}C$ system. Elastic scattering was first measured by Helb *et al.*[11] up to $E_{c.m.} = 14$ MeV. Korotky *et al.*[12] gave experimental data for the elastic scattering up to $E_{c.m.} = 35.5$ MeV and data for the transfer reaction $^{13}C(^{13}C,^{12}C)^{14}C$ in the energy range $E_{c.m.} = 8$–25 MeV. More recently, Balamuth *et al.*[13] presented experimental differential cross sections for the single and mutual excitation of the predominantly excited first $\frac{1}{2}^+$ state ($E^* = 3.09$ MeV) of ^{13}C.

Korotky *et al.*[12] carried out one-step distorted-wave Born approximation (DWBA) calculations of the differential cross section for the transfer reaction which could not reproduce the observed gross structures as function of energy. In contrast, the calculations of Könnecke *et al.*[8] using the molecular particle-core model showed better agreement with the transfer data. Balamuth *et al.*[13] claimed the failure of the molecular particle-core model, comparing their measured cross section for the mutual excitation of the first $\frac{1}{2}^+$ state of ^{13}C with the calculated one of Terlecki *et al.*[7] The measured cross section for the mutual excitation resulted about 25 times smaller than the predicted one. The calculations of Terlecki *et al.*[7] were at that time based on the only available elastic scattering data of Helb *et al.*[11] which went up only to $E_{c.m.} = 14$ MeV. In this paper we will show that a modified optical potential in the entrance $^{13}C + ^{13}C$ channel leads to the correct inelastic and transfer cross sections. Therefore, a shortcoming of the molecular particle-core model can not be maintained, as stated misleadingly by Balamuth *et al.*[13]

The aim of this paper is a comprehensive study of the scattering of ^{13}C on ^{13}C in the framework of the particle-core model. In Sec. II the existent formulation of the particle-core model[6,7] is extended to the inclusion of the one-nucleon transfer channels. In Sec. III we compare the results of coupled channel calculations for the inelastic excitation and neutron transfer with the experimental data. We will show that the transfer cross section is mainly caused by rotational coupling to the elastic channel which arises due to the molecular character of the single-particle wave functions used for the extra nucleons.

II. THE MOLECULAR MODEL FOR EXCITATION AND TRANSFER

On the basis of the work of Park *et al.*,[5] Terlecki *et al.*[7] formulated the particle-core model for the descrip-

tion of two colliding ^{13}C nuclei in terms of two ^{12}C cores with loosely bound neutrons. These neutrons can be excited by the coupling of the single-particle motion to the relative motion of the nuclear centers. Later Park *et al.*[6] considered the nucleon transfer for a system consisting of two cores and one valence nucleon. In the following we want to point out the modifications of the theory arising from the combined treatment of the excitation and transfer of the valence neutrons.

A. The Hamiltonian

According to the particle-core model the system, we consider, consists of two ^{12}C cores and two extra neutrons, described by molecular single-particle wave functions. If $s=0$ denotes the $^{13}C+{}^{13}C$ system and $s=1$ the $^{12}C+{}^{14}C$ system, the Hamiltonian for the fragmentation s is assumed to be as

$$H(s)=T_s+U_s+iW_s+H_{\text{s.p.}}+V_{\text{res}} , \tag{1}$$

where

$$T_s=-\frac{\hbar^2}{2\mu_s}\frac{1}{R_s^2}\left[\frac{\partial}{\partial R_s}+D_s\right]R_s^2\left[\frac{\partial}{\partial R_s}+D_s\right]+\frac{1}{2\mu_s R_s^2}[\mathbf{I}(\phi_s,\theta_s,\psi_s)-\mathbf{J}_s]^2$$
$$-\frac{1}{2A_1^{(s)}M}\left[\sum_{i=1}^{N_1^{(s)}}\mathbf{p}'_{i\text{c.m.}}\right]^2-\frac{1}{2A_2^{(s)}M}\left[\sum_{i=N_1^{(s)}+1}^{N}\mathbf{p}'_{i\text{c.m.}}\right]^2 , \tag{1a}$$

$$D_s=\frac{1}{A}\left[A_2^{(s)}\sum_{i=1}^{N_1^{(s)}}\frac{\partial}{\partial z'_{i\text{c.m.}}}-A_1^{(s)}\sum_{i=N_1^{(s)}+1}^{N}\frac{\partial}{\partial z'_{i\text{c.m.}}}\right] , \tag{1b}$$

$$\mathbf{J}_s=\sum_{i=1}^{N_1^{(s)}}\left(\mathbf{r}'_{i\text{c.m.}}-\frac{A_2^{(s)}}{A}\mathbf{R}_s\right)\times\mathbf{p}'_{i\text{c.m.}}+\sum_{i=N_1^{(s)}+1}^{N}\left[\mathbf{r}'_{i\text{c.m.}}+\frac{A_1^{(s)}}{A}\mathbf{R}_s\right]\times\mathbf{p}'_{i\text{c.m.}}+\sum_{i=1}^{2}\mathbf{s}'_i , \tag{1c}$$

$$H_{\text{s.p.}}=\sum_{i=1}^{2}h_{\text{TCSM}}(i)=\sum_{i=1}^{2}\frac{\mathbf{p}'^2_{i\text{c.m.}}}{2M}+V_{\text{TCSM}}(\mathbf{r}'_{i\text{c.m.}},\mathbf{p}'_{i\text{c.m.}},\mathbf{s}'_i,R_s)-E^{(s)}_{\text{g.s.}}(R_s) . \tag{1d}$$

The Hamiltonian (1) is written with respect to a rotating coordinate system, denoted by dashed coordinates, with the z' axis in the direction of the relative coordinate $\mathbf{R}_s$ between the nuclei. The Euler angles ϕ_s, θ_s (spherical polar angles of $\mathbf{R}_s$), and ψ_s (superfluous and unphysical third Euler angle) define the coordinate axes of the molecular system with respect to the laboratory system. The single particle coordinates $\mathbf{r}'_{i\text{c.m.}}$, momenta $\mathbf{p}'_{i\text{c.m.}}$, and spins $\mathbf{s}'_i$ are referred to the rotating coordinate system. The coordinates are measured with respect to the total center of mass. The numbers of nucleons in the two nuclei are $A_1^{(s)}$ and $A_2^{(s)}$ with $A_1^{(s)}+A_2^{(s)}=A$ and the numbers of extra particles $N_1^{(s)}$ and $N_2^{(s)}$ with $N_1^{(s)}+N_2^{(s)}=N$, where N is 2 in the case of the systems $^{13}C+{}^{13}C$ and $^{12}C+{}^{14}C$. The reduced mass in the fragmentation s is denoted by μ_s and the nucleon mass by M.

The operator of the kinetic energy consists of the expression (1a) and the kinetic energies of the extra nucleons in $H_{\text{s.p.}}$ (1d). It can be derived with a canonical transformation of the coordinates and momenta leading from the laboratory system to the rotating system, as shown in Refs. 6 and 7. The expression (1a) contains the radial and angular momentum parts (first and second terms) and correction terms due to the center-of-mass motion of the extra nucleons. The radial and angular momentum parts lead to the radial and rotational couplings between the different channels in the coupled equations (see Sec. II C). The operator D_s appearing in the radial term and given in Eq. (1b) ensures that for large separations of the nuclei the radial kinetic energy cannot induce any transitions in the nuclei. The rotational kinetic energy in Eq. (1a) contains the total angular momentum operator $\mathbf{I}$ depending on the Eulerian angles and the angular momentum operators $\mathbf{J}_s$ of the extra particles measured with respect to the centers of the individual nuclei. The operator $\mathbf{J}_s$ is defined in Eq. (1c). The third and fourth terms in Eq. (1a) will be neglected because the number $N=2$ of extra nucleons is small compared to the number of nucleons of the cores.

The Hamiltonian (1) contains an optical potential U_s+iW_s which depends on the relative coordinate. This complex potential should describe the mean interaction between the nuclei in the fragmentation s. Besides the very restricted number of reaction channels considered explicitly in this work, many other channels contribute during a collision. For an averaged description of all these channels which are not explicitly taken into account, one can use optical potentials describing the elastic scattering of ^{13}C on ^{13}C and of ^{12}C on ^{14}C. In the calculations we have taken the elastic $^{13}C+{}^{13}C$ optical potential for both fragmentations and added the experimental Q value to the potential in the case of the $^{12}C+{}^{14}C$ fragmentation.

In the TCSM Hamiltonian (1d) for the extra nucleons we subtract the R_s-dependent energy of the ground state of the valence neutrons because the excitation energy of these nucleons is measured with respect to the real part U_s of the optical potential. For simplicity, we use the

same TCSM for both fragmentations $s=0$ and 1 with the two-center potential of $^{13}C+^{13}C$. We assume that the extra nucleons move in the mean field generated by all nucleons. The residual interaction V_{res} between the extra nucleons is only accounted for in the extent that we use the experimental asymptotic Q value of $Q=3.23$ MeV in the transfer fragmentation.

B. The wave functions

For the wave functions solving the stationary scattering problem we take the ansatz of Ref. 5, namely

$$\Psi_{IM}=\mathcal{A}(1,2)\sum_{s,\alpha,l,J} R_{s\alpha lJI}(R_s)[i^l Y_l(\theta_s,\phi_s) \otimes \Phi_{s\alpha J}(1,2,\mathbf{R}_s)]^{[I]}_M \ . \quad (2)$$

The wave functions $R_{s\alpha lJI}(R_s)$ describe the radial relative motion of the colliding nuclei and depend on the fragmentation s and the quantum numbers of the total angular momentum I, the orbital angular momentum l and the channel spin J. With α we denote the various molecular single-particle configurations described by the wave functions $\Phi_{s\alpha J}$. Since we restrict this study to unexcited ^{12}C cores, we do not explicitly write down their intrinsic wave functions. The wave functions $\Phi_{s\alpha J}$ depend on the coordinates of the two valence neutrons and the relative distance $\mathbf{R}_s$. The operator $\mathcal{A}(1,2)$ antisymmetrizes the wave function for the exchange of the two valence neutrons. The wave function is symmetric with respect to the exchange of the ^{12}C cores.

The transformation of the wave function $\Phi_{s\alpha J}$ to the rotating coordinate system is given via the relation[14]

$$\Phi_{s\alpha JM}=\sum_{M'} D^{J*}_{MM'}(\phi_s,\theta_s,\psi_s)\tilde{\Phi}_{s\alpha(J)M'} \ . \quad (3)$$

This leads to

$$\Psi_{IM}=\sum_{s,\alpha,l,J}\left[\frac{2l+1}{8\pi^2}\right]^{1/2} i^l R_{s\alpha lJI}(R_s) \times\sum_{M'}(l0JM' \mid IM')D^{I*}_{MM'}(\phi_s,\theta_s,\psi_s)\tilde{\Phi}^{\mathcal{A}}_{s\alpha(J)M'} \ , \quad (4)$$

where

$$\tilde{\Phi}^{\mathcal{A}}_{s\alpha(J)M}=\mathcal{A}(1,2)\tilde{\Phi}_{s\alpha(J)M} \ . \quad (5)$$

A factor $(2\pi)^{-1/2}$ is included in Eq. (4) in order to account for the integration over the irrelevant Euler angle ψ_s in all matrix elements. The effect of the antisymmetrization operator $\mathcal{A}(1,2)$ on the relative coordinate $\mathbf{R}_s$ is small and, therefore, neglected in Eq. (4) by commuting $\mathcal{A}(1,2)$ with the $\mathbf{R}_s$-dependent factors of the wave function (2).

The functions $\tilde{\Phi}_{s\alpha(J)M}$ are built up by ortho-normalized single-particle wave functions $\phi_{\lambda(j)m}(\mathbf{r}'_{c.m.},\pm R_s/2)$ centered about $z'=\pm R_s/2$, namely

$$\tilde{\Phi}_{s\alpha(J)M}\propto\left\{\phi_{\alpha_1}\left[\mathbf{r}'_{1c.m.},\frac{R_s}{2}\right]\otimes\phi_{\alpha_2}\left[\mathbf{r}'_{2c.m.},(-1)^{s+1}\frac{R_s}{2}\right]\right\}^{[J]}_M \quad (6)$$

with the abbreviations $\alpha_i=\{\lambda_i(j_i)\}$, $\alpha=\{\alpha_1,\alpha_2\}$. The single-particle spins are only good quantum numbers for large separations which is indicated by the parentheses around j and J. With λ we denote the other quantum numbers of the occupied single-particle states. The functions $\phi_{\lambda(j)m}$ are the eigenfunctions of the Hamiltonian (1d) when the asymmetric TCSM is applied. Since in this work we use the symmetric TCSM, we have to combine the eigensolutions χ^g and χ^u of the symmetric TCSM Hamiltonian with even (g) and odd (u) parities in order that the basis functions are centered at the individual centers for large separations:

$$\phi_{\lambda(j)m}(\mathbf{r}',R_s/2)=\frac{1}{\sqrt{2}}[\chi^g_{\lambda(j)m}(\mathbf{r}')+\chi^u_{\lambda(j)m}(\mathbf{r}')] \ , \quad (7a)$$

$$\phi_{\lambda(j)m}(\mathbf{r}',-R_s/2)=\frac{(-1)^{l_\alpha}}{\sqrt{2}}[\chi^g_{\lambda(j)m}(\mathbf{r}')-\chi^u_{\lambda(j)m}(\mathbf{r}')] \ . \quad (7b)$$

The phases of the wave functions χ^g and χ^u are chosen by the condition that χ^g and χ^u become equal for $R\to\infty$ and $z'>0$. The phase factor $(-1)^{l_\alpha}$ in equation (7b) is the parity of the asymptotic single-particle wave function $\phi_{\lambda(j)m}(\mathbf{r}',\pm R_s/2)$ with respect to the centers at $z'=\pm R_s/2$. Here, l_α denotes the asymptotic quantum number of the orbital angular momentum (For further details see Ref. 7.).

The wave function Ψ_{IM} consists of four parts, namely the direct terms and terms generated by the exchange of the identical ^{12}C cores and the antisymmetrization of the extra particles. This leads to the following expression for the intrinsic wave function derived by the methods given in Refs. 6 and 7:

$$\tilde{\Phi}^{\mathcal{A}}_{s\alpha(J)M}(1,2,R_s)=\frac{1}{2(1+\delta_{\alpha_1\alpha_2})^{1/2}}\mathcal{A}(1,2)\left\{\phi_{\alpha_1}\left[\mathbf{r}'_{1c.m.},\frac{R_s}{2}\right]\otimes\phi_{\alpha_2}\left[\mathbf{r}'_{2c.m.},(-1)^{s+1}\frac{R_s}{2}\right]-(-1)^l\phi_{\alpha_1}\left[\mathbf{r}'_{2c.m.},\frac{-R_s}{2}\right]\otimes\phi_{\alpha_2}\left[\mathbf{r}'_{1c.m.},(-1)^s\frac{R_s}{2}\right]\right\}^{[J]}_M \quad (8)$$

with the normalization

$$\langle\tilde{\Phi}^{\mathcal{A}}_{s\alpha l(J)M}\mid\tilde{\Phi}^{\mathcal{A}}_{s'\alpha' l'(J')M'}\rangle=\frac{1+(-1)^{l+l'}}{2(1+\delta_{\alpha_1\alpha_2})}\delta_{ss'}\delta_{JJ'}\delta_{MM'}[\delta_{\alpha_1\alpha'_1}\delta_{\alpha_2\alpha'_2}-(-1)^{l(s+1)+j_1+j_2-J}\delta_{\alpha_1\alpha'_2}\delta_{\alpha_2\alpha'_1}] \ . \quad (9)$$

C. The coupled equations

The coupled equations are obtained by projection of the stationary Schrödinger equation $H\Psi=E\Psi$ on the channel wave functions. Since the Hamiltonian (1) and the wave functions (2) depend on the fragmentation s we proceed in the same way as suggested in Ref. 6. At first we divide the wave function with respect to the fragmentation

$$\Psi_{IM}=\sum_{K(s=0)}\frac{1}{R_{s=0}}u_{K(s=0)I}(R_{s=0})\psi^{A}_{K(s=0)IM}+\sum_{K(s=1)}\frac{1}{R_{s=1}}u_{K(s=1)I}(R_{s=1})\psi^{A}_{K(s=1)IM}\ , \tag{10}$$

where

$$\psi^{A}_{K(s)IM}=\left[\frac{2l+1}{8\pi^2}\right]^{1/2}\sum_{M'}(l0JM'\mid IM')D^{I*}_{MM'}\tilde{\Phi}^{A}_{K(s)M'}\ , \tag{11a}$$

$$u_{K(s)I}(R_s)=i^{l}R_sR_{K(s)I}(R_s)\ , \tag{11b}$$

$$K=\{s\alpha lJ\}\ . \tag{11c}$$

Then the projection yields for a given total angular momentum I the following system of coupled equations for the radial functions:

$$\sum_{K'(s)}D_{K(s),K'(s)}(R_s)u_{K'(s)I}(R_s)+\sum_{K'(\bar{s})}D_{K(s),K'(\bar{s})}(R_s)u_{K'(\bar{s})I}(R_s)=0\ , \tag{12}$$

where $s=0$ or 1 and $\bar{s}\neq s$. The matrix elements are operators and obtained as

$$D_{K(s),K'(s)}=\int\psi^{*}_{K(s)IM}(\mathbf{r}'_{1\text{c.m.}},\mathbf{r}'_{2\text{c.m.}},\mathbf{R}_s)[H(s,\mathbf{R}_s)-E]\psi^{A}_{K'(s)IM}(\mathbf{r}'_{1\text{c.m.}},\mathbf{r}'_{2\text{c.m.}},\mathbf{R}_s)d^3r'_{1\text{c.m.}}d^3r'_{2\text{c.m.}}d\Omega_s\ , \tag{13a}$$

$$D_{K(s),K'(\bar{s})}u_{K'(\bar{s})I}=\int\psi^{*}_{K(s)IM}(\mathbf{r}'_{1\text{c.m.}},\mathbf{r}'_{2\text{c.m.}},\mathbf{R}_s)[H(s,\mathbf{R}_s)-E]\psi^{A}_{K'(\bar{s})IM}(\mathbf{r}'_{1\text{c.m.}},\mathbf{r}'_{2\text{c.m.}},\mathbf{R}_{\bar{s}})u_{K'(\bar{s})I}(R_{\bar{s}})d^3r'_{1\text{c.m.}}d^3r'_{2\text{c.m.}}d\Omega_s\ , \tag{13b}$$

where $H(s,\mathbf{R}_s)$ is the Hamiltonian (1). Since we neglect the recoil effects in the following, i.e., the differences in the coordinates $\mathbf{R}_{s=0}$ and $\mathbf{R}_{s=1}$, which are small, we can set $\mathbf{R}_{s=0}=\mathbf{R}_{s=1}=\mathbf{R}$. In this case the radial wave function $u_{K'(\bar{s})I}$ in Eq. (13b) can be traced out of the integral. The matrix elements are not Hermitian if we disregard the recoil effects and the third and fourth terms of the kinetic energy (1a). In order to ensure the Hermitian properties of the coupled equations (12) (besides the imaginary potentials W_s), we add the Hermitian conjugated terms in Eqs. (13a) and (13b). In this connection the Hamiltonian in Eq. (13b) has to be replaced by the average over $s=0$ and 1 (for details see Ref. 6):

$$H(s,\mathbf{R}_s)\rightarrow\tfrac{1}{2}[H(s=0,\mathbf{R})+H(s=1,\mathbf{R})]\ . \tag{14}$$

The matrix elements (13a) are given by

$$D_{K(s),K'(s)}=\delta_{K(s),K'(s)}\left[-\frac{\hbar^2}{2\mu_s}\frac{d^2}{dR^2}+U_s+iW+\epsilon_{K(s)}-E\right]$$
$$+\sum_{M',M''}(-1)^{l-l'+M''-M'}(IM'J-M'\mid l0)(IM''J'-M''\mid l'0)\left[-\frac{\hbar^2}{2\mu_s}\delta_{M'M''}C^{\text{rad}}_{K(s),K'(s)}(s)+\frac{1}{2\mu_sR^2}C^{\text{rot}}_{K(s),K'(s)}(s)\right] \tag{15}$$

with

$$\epsilon_{K(s)}=\delta_{MM'}\left\langle\tilde{\Phi}^{A}_{K(s)M}\left|\sum_{i=1}^{2}h_{\text{TCSM}}\right|\tilde{\Phi}^{A}_{K(s)M'}\right\rangle\quad\text{for } j_1=j_2=\tfrac{1}{2}\ , \tag{16}$$

$$C^{\text{rad}}_{K(s),K'(s')}(s'')=\left\langle\tilde{\Phi}_{K(s)}\left|\left[\frac{\partial}{\partial R}+D_{s''}\right]^2\right|\tilde{\Phi}^{A}_{K'(s')}\right\rangle+\text{H.c.}+2\left\langle\tilde{\Phi}_{K(s)}\left|\left[\frac{\partial}{\partial R}+D_{s''}\right]\right|\tilde{\Phi}^{A}_{K'(s')}\right\rangle\frac{d}{dR}+\text{H.c.}\ , \tag{17}$$

$$C^{\text{rot}}_{K(s),K'(s')}(s'')=\frac{2I+1}{8\pi^2}\langle D^{I*}_{MM'}\tilde{\Phi}^{A}_{K(s)M'}\mid(\mathbf{I}-\mathbf{J}_{s''})^2\mid D^{I*}_{MM''}\tilde{\Phi}^{A}_{K'(s')M''}\rangle\ . \tag{18}$$

In the transfer matrix elements (13b) the Hamiltonian $H(s,\mathbf{R}_s)$ is replaced by the expression (14). They are obtained as

$$D_{K(s),K'(\bar{s})}=\sum_{M',M''}(-1)^{l-l'+M''-M'}(IM'J-M'\mid l0)(IM''J'-M''\mid l'0)$$
$$\times\left\{-\frac{\hbar^2}{4}\delta_{M'M''}\left[\frac{1}{\mu_{s=0}}C^{\rm rad}_{K(s),K'(\bar{s})}(s''=0)+\frac{1}{\mu_{s=1}}C^{\rm rad}_{K(s),K'(\bar{s})}(s''=1)\right]\right.$$
$$\left.+\frac{1}{4R^2}\left[\frac{1}{\mu_{s=0}}C^{\rm rot}_{K(s),K'(\bar{s})}(s''=0)+\frac{1}{\mu_{s=1}}C^{\rm rot}_{K(s),K'(\bar{s})}(s''=1)\right]\right\}. \tag{19}$$

Inserting (15) and (19) into (12) and multiplying (12) by $2\mu_s/\hbar^2$ we note that the resulting system of coupled equations is not exactly—but in good approximation—Hermitian because the ratio of the reduced masses μ_0/μ_1 appearing in the transfer terms (19) is not exactly 1 ($\mu_0/\mu_1=1.006$).

The evaluation of the radial coupling matrix elements (17) results in the following expressions

$$C^{\rm rad}_{K(s),K'(s')}(s''=0)=4\left[\langle\tilde{\Phi}_{K(s)}(1,2,R)\mid D_0\mid\tilde{\Phi}_{K'(s')}(1,2,R)\rangle+\left\langle\tilde{\Phi}_{K(s)}(1,2,R)\left|\frac{\partial}{\partial R}\right|\tilde{\Phi}^{A}_{K'(s')}(1,2,R)\right\rangle\right]\frac{d}{dR}$$
$$+2\left\langle\tilde{\Phi}_{K(s)}(1,2,R)\left|\frac{\partial^2}{\partial R^2}+D_0^2\right|\tilde{\Phi}^{A}_{K'(s')}(1,2,R)\right\rangle+4\left\langle\tilde{\Phi}_{K(s)}(1,2,R)\left|\frac{\partial}{\partial R}D_0\right|\tilde{\Phi}_{K'(s')}(1,2,R)\right\rangle, \tag{20a}$$

$$C^{\rm rad}_{K(s),K'(s')}(s''=1)=4\left\langle\tilde{\Phi}_{K(s)}(1,2,R)\left|\frac{\partial}{\partial R}+D_1\right|\tilde{\Phi}^{A}_{K'(s')}(1,2,R)\right\rangle\frac{d}{dR}+2\left\langle\tilde{\Phi}_{K(s)}(1,2,R)\left|\frac{\partial^2}{\partial R^2}+D_1^2\right|\tilde{\Phi}^{A}_{K'(s')}(1,2,R)\right\rangle$$
$$+4\left\langle\tilde{\Phi}_{K(s)}(1,2,R)\left|\frac{\partial}{\partial R}D_1\right|\tilde{\Phi}^{A}_{K'(s')}(1,2,R)\right\rangle. \tag{20b}$$

Here we used the following relations in constructing the matrix elements (20a) and (20b) as Hermitian

$$\langle\tilde{\Phi}_{K(s)}(1,2,R)\mid D_0\mid\tilde{\Phi}^{A}_{K'(s')}(1,2,R)\rangle+\langle\tilde{\Phi}^{A}_{K(s)}(1,2,R)\mid D_0\mid\tilde{\Phi}_{K'(s')}(1,2,R)\rangle=2\langle\tilde{\Phi}_{K(s)}(1,2,R)\mid D_0\mid\tilde{\Phi}_{K'(s')}(1,2,R)\rangle, \tag{21a}$$

$$\langle\tilde{\Phi}_{K(s)}(1,2,R)\mid D_1\mid\tilde{\Phi}^{A}_{K'(s')}(1,2,R)\rangle+\langle\tilde{\Phi}^{A}_{K(s)}(1,2,R)\mid D_1\mid\tilde{\Phi}_{K'(s')}(1,2,R)\rangle=2\langle\tilde{\Phi}_{K(s)}(1,2,R)\mid D_1\mid\tilde{\Phi}^{A}_{K'(s')}(1,2,R)\rangle. \tag{21b}$$

The matrix elements (20a) and (20b) can be rearranged into two terms which are individually Hermitian

$$C^{\rm rad}_{K(s),K'(s')}(s'')=A_{K(s),K'(s')}(s'')+B_{K(s),K'(s')}(s'') \tag{22}$$

with

$$A_{K(s),K'(s')}(s'')=2M_{K(s),K'(s')}(s'')\frac{d}{dR}+\frac{d}{dR}[M_{K(s),K'(s')}(s'')], \tag{23}$$

$$M_{K(s),K'(s')}(s''=0)=2\left[\left\langle\tilde{\Phi}_{K(s)}(1,2,R)\mid D_0\mid\tilde{\Phi}_{K'(s')}(1,2,R)\right\rangle+\left\langle\tilde{\Phi}_{K(s)}(1,2,R)\left|\frac{\partial}{\partial R}\right|\tilde{\Phi}^{A}_{K'(s')}(1,2,R)\right\rangle\right], \tag{23a}$$

$$M_{K(s),K'(s')}(s''=1)=2\left\langle\tilde{\Phi}_{K(s)}(1,2,R)\left|\frac{\partial}{\partial R}+D_1\right|\tilde{\Phi}^{A}_{K'(s')}(1,2,R)\right\rangle, \tag{23b}$$

and

$$B_{K(s),K'(s')}(s'')=-2\left[\left\langle D_{s''}\tilde{\Phi}^{A}_{K(s)}(1,2,R)\left|\frac{\partial}{\partial R}+D_{s''}\right|\tilde{\Phi}_{K'(s')}(1,2,R)\right\rangle\right.$$
$$\left.+\left\langle\frac{\partial}{\partial R}\tilde{\Phi}_{K(s)}(1,2,R)\left|\frac{\partial}{\partial R}+D_{s''}\right|\tilde{\Phi}^{A}_{K'(s')}(1,2,R)\right\rangle+\delta_{s''0}\frac{d}{dR}[\langle\tilde{\Phi}_{K(s)}(1,2,R)\mid D_0\mid\tilde{\Phi}_{K'(s')}(2,1,R)\rangle]\right]. \tag{24}$$

If we restrict our considerations only to the elastic and inelastic $^{13}C+{}^{13}C$ channels, these equations reduce to those given in Ref. 7 because in this case the following matrix elements of the operators D_0 or $\partial/\partial R$ vanish:

$$\left\langle\tilde{\Phi}_{K(0)}(1,2,R)\left|D_0\ \text{ or }\ \frac{\partial}{\partial R}\right|\tilde{\Phi}_{K'(0)}(2,1,R)\right\rangle=0. \tag{25}$$

The radial transfer matrix elements of the operators D_s and $\partial/\partial R$ between single-particle states located at different nuclear centers approach zero at large relative distances when the same TCSM is used for both fragmentations.

The rotational matrix elements can be reduced into the form

$$C^{\mathrm{rot}}_{K(s)M',K'(s')M''}(s'')=\delta_{M''M'}\delta_{JJ'}\frac{1+(-1)^{l+l'}}{2}\delta_{\alpha\alpha'}\hbar^2 I(I+1)-\hbar[I(I+1)+M''(1-M'')]^{1/2}\delta_{M',M''-1}\langle\tilde{\Phi}^{A}_{KM''-1}\,|\,J_{s''}^{-}\,|\,\tilde{\Phi}^{A}_{K'M''}\rangle$$

$$-\hbar[I(I+1)-M''(1+M'')]^{1/2}\delta_{M',M''+1}\langle\tilde{\Phi}^{A}_{KM''+1}\,|\,J_{s''}^{+}\,|\,\tilde{\Phi}^{A}_{K'M''}\rangle$$

$$-2\hbar M'\delta_{M'M''}\langle\tilde{\Phi}^{A}_{KM'}\,|\,J_{zs''}\,|\,\tilde{\Phi}^{A}_{K'M'}\rangle+\delta_{M'M''}\langle\tilde{\Phi}^{A}_{KM'}\,|\,\mathbf{J}^2_{s''}\,|\,\tilde{\Phi}^{A}_{K'M'}\rangle\ . \tag{26}$$

We note that

$$\lim_{R\to\infty}\mathbf{J}_s^2\tilde{\Phi}_{K(s)M}=\hbar^2 J(J+1)\tilde{\Phi}_{K(s)M}\ . \tag{27}$$

In the actual calculations of the matrix elements (26) the orbital angular momentum part of the operator $\mathbf{J}_s$ is replaced by expressions used in the TCSM for the diagonalization of the spin-orbit coupling and l^2 terms (see Ref. 7). Since these TCSM matrix elements are already properly symmetrized, the matrix elements (26) are obtained as Hermitian.

III. APPLICATION TO THE ^{13}C+^{13}C SCATTERING

For the application of the particle-core model we have selected the $^{13}C + {}^{13}C$ system. Here we consider the elastic and inelastic scattering and the neutron transfer to the $^{12}C + {}^{14}C$ system. The ^{13}C nucleus is described by a ^{12}C core and a neutron and the ^{14}C nucleus by the same core with two neutrons. The neutron occupies the $1p_{1/2}$ state in the ^{13}C ground state. As inelastic channels we take the single and mutual excitation of the first $\frac{1}{2}^+$ state of ^{13}C at $E^*=3.09$ MeV which is connected by a strong $E1$ transition with the ground state. The first $\frac{1}{2}^+$ state of ^{13}C can be described by the excitation of the neutron to the $2s_{1/2}$ state. The transfer channel is assumed as the g.s.-g.s. configuration of the $^{12}C + {}^{14}C$ system. The ground state of ^{14}C consists of a ^{12}C core with two neutrons bound in the $1p_{1/2}$ state and coupled to spin zero. First we specify the diagonal optical potential and the parameters of the TCSM for the description of the valence neutrons in terms of molecular TCSM wave functions. Then we present the results of the coupled channel calculations.

A. The optical potential

As optical potential we use that obtained by Korotky *et al.*[12] which they applied to describe the measured $^{13}C + {}^{13}C$ elastic cross section as function of the incident energy (excitation function). Analyzing the optical model calculation these authors showed that the gross structure of the calculated elastic excitation function could also be generated by the barrier top model of Friedman and Goebel.[15] In this model a barrier of the real potential with strong absorption behind it leads to the occurrence of barrier resonances closely related to the classical notion of orbiting. This interpretation of $^{13}C + {}^{13}C$ elastic scattering gross structure in terms of an orbiting phenomenon is also found in the heavier system $^{28}Si + {}^{28}Si$.[16]

B. The TCSM for the valence neutrons and the coupling potentials

As in the paper of Terlecki *et al.*,[7] the valence neutrons are described as asymptotically occupying the $1p_{1/2}$ and $2s_{1/2}$ levels. The $2s_{1/2}$ level of ^{13}C lies energetically below the $1d_{5/2}$ level. The TCSM parameters were adjusted in order that they reproduce these single particle states of ^{13}C near the Fermi level at large internuclear distances. We set the TCSM parameters $\hbar\omega_\infty=6.95$ MeV, $\kappa_\infty=0.127$, $\mu_\infty=-0.479$, which are the same as used by Terlecki *et al.*[7] The neck parameter of the TCSM,[4] which defines the ratio of the barrier height of the actual TCSM potential to that of the two-center oscillator, was set to $\epsilon=1$. Therefore, the two fragments have spherical

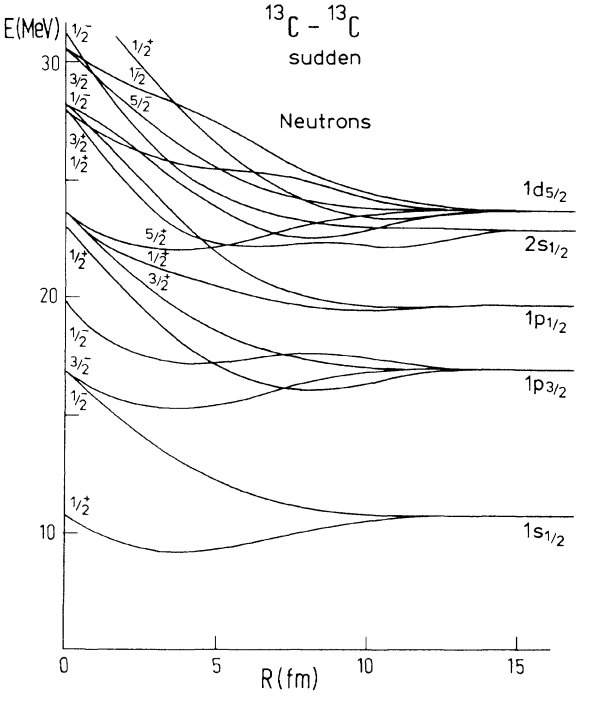

FIG. 1. The TCSM level diagram for neutron states of the system $^{13}C + {}^{13}C \rightarrow {}^{26}Mg$. The level diagram is calculated in the sudden approximation with the parameters $\hbar\omega=6.95$ MeV, $\kappa=0.127$, $\mu=-0.479$, and $\epsilon=1$. It is used in both fragmentations. In the actual calculations we consider the $1p_{1/2}$ and $2s_{1/2}$ levels.

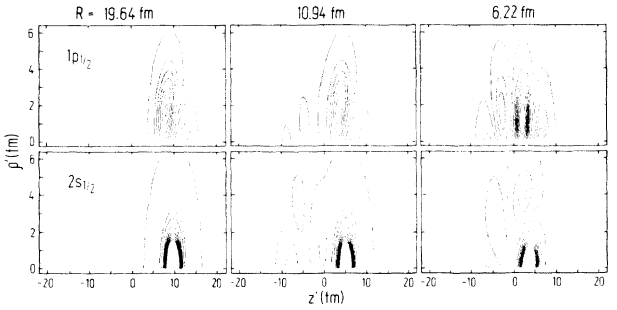

FIG. 2. Contour plots of the density distribution of a neutron, centered asymptotically at the core at the right hand side and occupying the $1p_{1/2}$ and $2s_{1/2}$ level, for the internuclear distances $R=19.64$, 10.94, and 6.22 fm. The equi-density curves are shown in the (ρ',z') plane $[\rho'=(x'^2+y'^2)^{1/2}]$.

shapes ("sharp" barrier) for all relative distances.

The TCSM calculations were carried out in the sudden approximation, i.e., the parameters $\hbar\omega$, κ, μ, and ϵ were assumed as independent of R. We note that the resulting cross sections remained unchanged when we used the TCSM in the adiabatic approximation with a value of the neck parameter of $\epsilon=0.85$. This independence on the type of the approximation proves that the relevant couplings occur for relative distances where the overlap of the collision partners is small.

Figure 1 shows the TCSM level diagram of neutron states for the system $^{13}C+{}^{13}C\rightarrow{}^{26}Mg$. As expected this symmetric system has no pronounced avoided level crossings as one observes them for example in the $^{13}C+{}^{16}O\rightarrow{}^{29}Si$ system (Park *et al.*[17]). In Fig. 2 we show the density of the molecular wave function $\phi_{\lambda(j)m}$ (see Sec. II B) of the $1p_{1/2}$ and $2s_{1/2}$ states for three different internuclear distances. One recognizes the increasing polarization of the $1p_{1/2}$ and $2s_{1/2}$ orbits with decreasing distance between the nuclei.

With the wave functions of the molecular $1p_{1/2}$ and $2s_{1/2}$ states we calculated the coupling potentials (23) and (26). The coupling potentials (24) were neglected in this work. Figure 3 shows some selected radial and rotational matrix elements for transfer. The polarization of the wave functions of the extra nucleons leads to a direct rotational coupling between the elastic and transfer channels. The rotational transfer matrix elements vanish for large relative distances because the wave functions have a good spin there [compare the inset of Fig. 3(b) with Fig. 2]. The rotational coupling between the elastic and transfer channels shown in Fig. 3(c) is stronger for odd partial waves than for even ones. As we will discuss in Sec. III D, the rotational coupling is mainly responsible for the feeding of the transfer channels since this coupling is stronger at large relative distances than the radial coupling.

C. Results of the coupled channel calculations

In Figs. 4–6 we show the elastic, inelastic and transfer excitation functions, obtained by solving the coupled

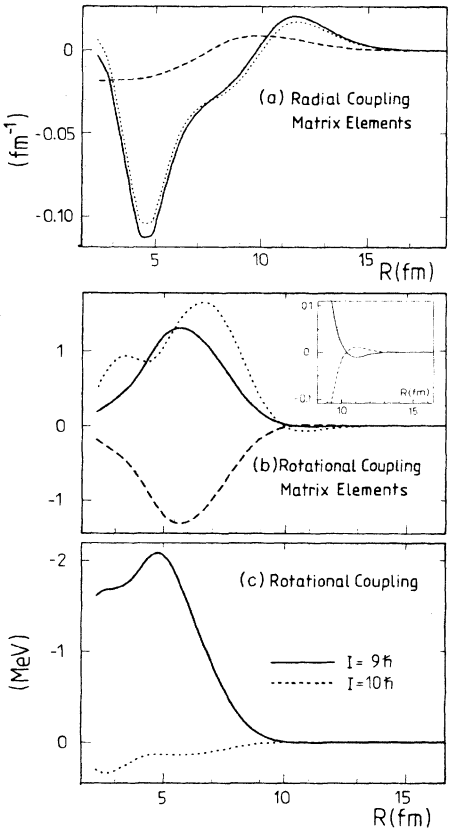

FIG. 3. (a) The radial coupling matrix elements $\langle\tilde{\Phi}_K\,|\,\partial/\partial R\,|\,\tilde{\Phi}_{K'}^{A}\rangle$ (dotted curve), $\langle\tilde{\Phi}_K\,|\,D_0\,|\,\tilde{\Phi}_{K'}\rangle$ (dashed curve), and $[M_{KK'}(s''=0)+M_{KK'}(s''=1)]/2$ (solid curve) [see Eqs. (23a) and (23b)] between the single inelastic channel $K=\{s=0,$ (g.s., $\frac{1}{2}^+$), $J=1,$ l odd$\}$ and transfer channel $K'=\{s=1,$ (g.s., g.s.), $J=0,$ l even$\}$. (b) The rotational coupling matrix elements between the elastic and transfer channels:

$$\text{(i)}\ \frac{1}{\hbar}\langle\tilde{\Phi}_{KM-1}^{A}\,|\,J^-\,|\,\tilde{\Phi}_{K'M}^{A}\rangle\ \text{(solid curve)}$$

and

$$\frac{1}{\hbar}\langle\tilde{\Phi}_{KM+1}^{A}\,|\,J^+\,|\,\tilde{\Phi}_{K'M}^{A}\rangle\text{(dashed curve)}$$

with $K=\{s=0,$ (g.s., g.s.), $J=1,$ l odd$\}$ and $K'=\{s=1,$ (g.s., g.s.), $J=0,$ l odd$\}$,

$$\text{(ii)}\ \frac{1}{\hbar^2}\langle\tilde{\Phi}_{KM}^{A}\,|\,J^2\,|\,\tilde{\Phi}_{K'M}^{A}\rangle\ \text{(dotted curve)}$$

with $K=\{s=0,$(g.s., g.s.), $J=0,$ l even$\}$ and $K'=\{s=1,$ (g.s. g.s.), $J=0,$ l even$\}$. The calculation of these matrix elements is carried out as described after Eq. (27). The inset shows the onset of the matrix elements in the surface region. (c) Rotational coupling matrix element

$$\frac{1}{2\mu R^2}\langle(Y_l\otimes\Phi_{K(s=0)}^{A})^{[I]}\,|\,(\mathbf{I}-\mathbf{J})^2\,|\,[Y_{l'}\otimes\Phi_{K'(s=1)}^{A}]^{[I]}\rangle$$

between the elastic and transfer channels for the angular momenta $J_{s=0}=1$, $I=9$ (solid) and $J_{s=0}=0$, $I=10$ (dotted curve).

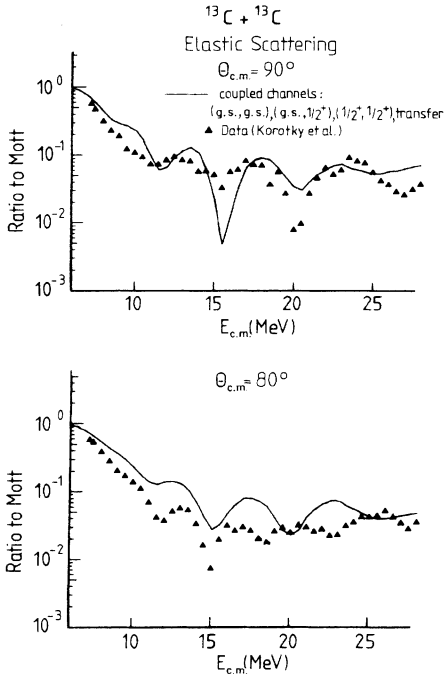

FIG. 4. The ratio to the Mott cross section for the elastic scattering of ^{13}C on ^{13}C at $\theta_{c.m.} = 90°$ and 80°. The solid curve is obtained by coupled channel calculations. The coupled channels are the elastic one, the single and mutual excitation of the first $\frac{1}{2}^+$ state of ^{13}C ($E^* = 3.09$ MeV), and the neutron transfer to the $^{12}C + ^{14}C$ system, where the ^{12}C and ^{14}C nuclei are in the ground state.

channel equations (12), in comparison with the experimental data of Korotky *et al.*[12] and Balamuth *et al.*[13] The calculations reproduce the main features of the data. The elastic excitation functions shown in Fig. 4 for $\theta_{c.m.} = 90°$ and 80° differ slightly from the uncoupled optical model calculations of Korotky *et al.*[12] The coupling damps some oscillations, and the first gross structure of

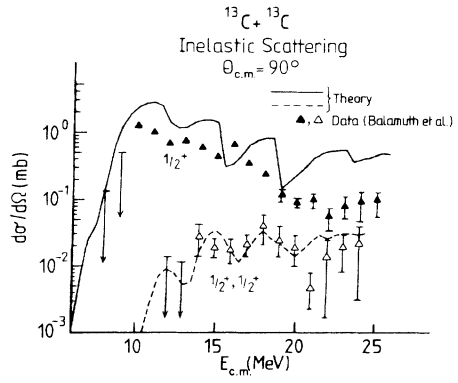

FIG. 5. The differential cross sections for the single and mutual excitation of the first $\frac{1}{2}^+$ state of ^{13}C in collisions of ^{13}C on ^{13}C at $\theta_{c.m.} = 90°$. The calculated cross sections are represented by solid and dashed curves. The triangles are the data of Balamuth *et al.* (Ref. 13).

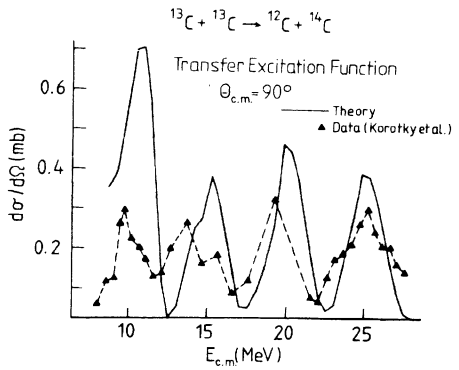

FIG. 6. The differential transfer cross section of the reaction $^{13}C + ^{13}C \rightarrow ^{12}C + ^{14}C$ at $\theta_{c.m.} = 90°$. The calculated cross section is shown by the solid curve. The triangles connected by a dashed line are the data of Korotky *et al.* (Ref. 12).

the 80° excitation function between 10 and 15 MeV is shifted towards higher energies in agreement with the data. The calculated single and double inelastic cross sections shown in Fig. 5 have the right order of magnitude. The pronounced structure of the single inelastic excitation function can probably be damped out via the coupling to other inelastic channels not considered so far.

The theoretical transfer excitation function shown in

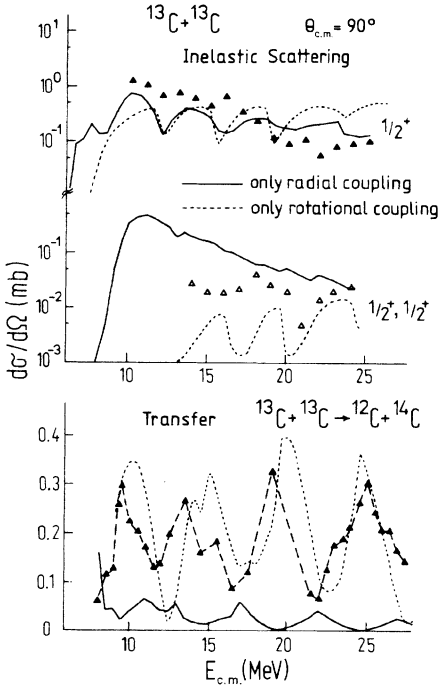

FIG. 7. The 90° excitation functions for the single and mutual excitation of the first $\frac{1}{2}^+$ state of ^{13}C and the neutron transfer reaction for ^{13}C on ^{13}C. The solid curves show the results of coupled channel calculations where only the radial couplings are used. The dashed curves give the results with only the rotational couplings used. The triangles denote data of Korotky *et al.* (Ref. 12) (neutron transfer) and Balamuth *et al.* (Ref. 13) (inelastic scattering).

Fig. 6 reveals the same oscillatory behavior as the data over the considered range of energies. This is in contrast to the one-step DWBA calculations of Korotky *et al.*[12] which yield a transfer excitation function without an energy-dependent structure. Figure 7 demonstrates the effects of the radial and rotational coupling terms. While both coupling types are equally important for the inelastic channels, the transfer channels are mainly fed by the rotational coupling between the elastic and transfer channels as calculations have shown with only these channels.

In the early calculations of Terlecki *et al.*,[7] it was found however that the radial coupling was the most important coupling for the inelastic channels. The difference between the present results and these early calculations arises due to the fact that Terlecki *et al.*[7] used a quite different optical potential. The barriers of their effective real potential were located at much smaller relative distances (5–6 fm) compared to the barrier radius (~8 fm) of the real potential used in this calculation. The absorption of their imaginary potential, adjusted to the radial position of the barrier of the real potential, set in at relative distances of 4–5 fm. Therefore, the radial coupling terms which are larger at these radial distances could act and fed the inelastic channels strongly.

D. Analysis of the excitation function for transfer

In this subsection we investigate the origin of the energy-dependent structure of the transfer excitation function. We remind that two types of transfer channels are present, namely those with odd and even orbital angular momenta l. Because of $J=0$ the orbital angular momentum of these channels is equal to the total angular momentum: $l=I$. The two types of transfer channels couple with different strengths to the elastic ones. The rotational coupling for odd angular momenta I arises from the Coriolis coupling and is large and proportional to $[I(I+1)]^{1/2}$. In contrast to this case the even angular momenta I have a smaller rotational coupling between these channels, resulting from nonvanishing matrix elements of the operator J^2 [see Figs. 3(b) and 3(c)]. Figure 8 shows the 90° excitation function for the neutron transfer obtained from a coupled channel calculation using only the elastic and transfer channels with odd or even total angular momenta, respectively. Comparing these results with the excitation function shown in Figs. 6 and 7 we conclude that the structures are obtained mainly due to the partial waves with odd total angular momenta.

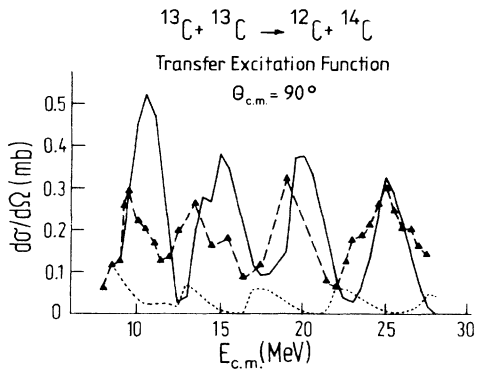

FIG. 8. The 90° excitation function for transfer calculated by coupling only the elastic and transfer channels. The solid curve is calculated with odd values of I and the dashed curve with even values of I only. The inelastic channels are not considered in this calculation. The data (triangles) are taken from Korotky *et al.* (Ref. 12).

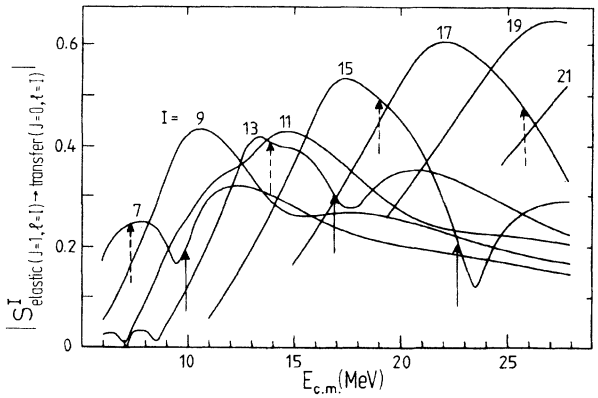

FIG. 9. The absolute value of the S-matrix elements $|S^I_{\text{elastic}(J=1,l=I),\text{transfer}(J=0,l=I)}|$ for angular momenta of 7–21 $\hbar$ as functions of energy. The solid and dashed arrows indicate the energies of the first virtual resonance states lying just above the barrier of the corresponding real effective potential of the elastic and transfer channels, respectively. No absorption or couplings to other channels are included in the calculation of the energies of the states.

Figure 9 shows the dominant S-matrix elements $|S^I_{\text{elastic}(J=1,l=I),\text{transfer}(J=0,l=I)}|$ for odd angular momenta from $I=7\hbar$ to $21\hbar$. Partial waves with angular momenta smaller than $7\hbar$ do not much contribute to the transfer cross section as calculations without these partial waves have shown. The solid and dashed arrows in Fig. 9

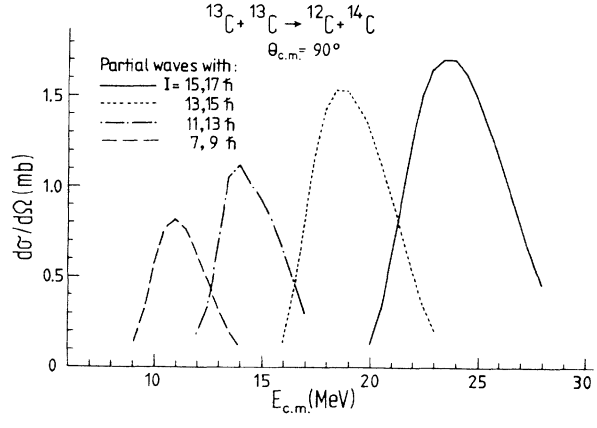

FIG. 10. The 90° transfer cross section calculated by coupling the elastic channels to the transfer channels only for two successive odd partial waves. The odd angular momenta are chosen in this manner that the corresponding S-matrix elements, shown in Fig. 9, have maxima and minima in the considered energy region. No inelastic channels are included.

indicate the energies of the first virtual resonance state lying just above the barriers of the potentials in the elastic and transfer channels, respectively. These states were obtained with effective real potentials which included the diagonal matrix elements (no coupling to other channels and no absorbing potentials). The structures of the S-matrix elements shown in Fig. 9 are correlated with these resonance states. For the angular momenta $9\hbar$ and $11\hbar$ we did not find virtual resonances lying near the top of the real potential barriers.

In Fig. 10 differential cross sections for transfer are displayed which are calculated with two successive odd partial waves only whose corresponding S-matrix elements have structures in the considered energy region (see Fig. 9). It is interesting to note that the superposition of two partial waves with successive odd angular momenta leads to smaller structures by a destructive interference in the transfer cross section. From Fig. 10 we conclude that each structure of the transfer cross section is produced by more than one partial wave with odd total angular momentum.

IV. CONCLUSIONS

In this paper we have shown for the $^{13}C + {}^{13}C$ system that a unified interpretation of the inelastic scattering data of Balamuth *et al.*[13] as well as the one-nucleon transfer data of Korotky *et al.*[12] is possible on the basis of the dynamical molecular particle-core model. The only ingredients are the optical potential for $^{13}C + {}^{13}C$ and the parameters of the TCSM which are determined by fitting the levels of ^{13}C about the Fermi level.

In this model the dominant mechanism for the transfer reaction $^{13}C(^{13}C,^{12}C)^{14}C$ is directly connected with the molecular character of the wave functions of the extra nucleons. The polarization of the valence orbitals leads to nonvanishing rotational couplings between the elastic and transfer channels. We found that the Coriolis coupling is the dominant one due to its dependence on the total angular momentum. The origin of the transfer gross structure is traced back to the interference of successive odd partial waves. The structures of the corresponding S-matrix elements are correlated with the occurrence of resonance states in the relative motion. These states lie just on top of the barriers of the real diagonal potential of the elastic and transfer channels.

In the present calculations we neglected recoil effects and modifications of the relative coordinate due to the antisymmetrization. This procedure is justified in view of the fact that the main contributions of the coupling potentials come from the surface region of the optical potential. In the surface region the overlap between the collision partners is small and, therefore, possible corrections arising from these terms should not play an essential role.

This work was supported by the Bundesministerium für Forschung und Technologie (BMFT) and the Gesellschaft für Schwerionenforschung (GSI).

[1]D. A. Bromley, J. A. Kuehner, and E. Almqvist, Phys. Rev. Lett. **4**, 365 (1960).
[2]B. Imanishi and W. von Oertzen, Institute for Nuclear Study, University of Tokyo Report No. 586, 1986.
[3]P. Holzer, U. Mosel, and W. Greiner, Nucl. Phys. **A138**, 241 (1969).
[4]J. Maruhn and W. Greiner, Z. Phys. **251**, 431 (1972).
[5]J. Y. Park, W. Scheid, and W. Greiner, Phys. Rev. C **6**, 1565 (1972).
[6]J. Y. Park, W. Scheid, and W. Greiner, Phys. Rev. C **20**, 188 (1979).
[7]G. Terlecki, W. Scheid, H.-J. Fink, and W. Greiner, Phys. Rev. C **18**, 265 (1978).
[8]R. Könnecke, W. Greiner, and W. Scheid, Phys. Rev. Lett. **51**, 366 (1983).
[9]W. von Oertzen and W. Nörenberg, Nucl. Phys. **A207**, 113 (1973).
[10]F. Becker, S. Joffily, C. Beccaria, and G. Baron, Nucl. Phys. **A221**, 475 (1974).
[11]H.-D. Helb, P. Dück, G. Hartmann, G. Ischenko, F. Siller, and H. Voit, Nucl. Phys. **A206**, 385 (1973).
[12]S. K. Korotky, K.A. Erb, R. L. Phillips, S. J. Willett, and D. A. Bromley, Phys. Rev. C **28**, 168 (1983).
[13]D. P. Balamuth, W. K. Wells, T. Chapuran, D. P. Bybell, and C. M. Laymon, Phys. Lett. **140B**, 295 (1984).
[14]J. M. Eisenberg and W. Greiner, *Nuclear Models* (North-Holland, Amsterdam, 1970), Vol. I.
[15]W. A. Friedman and C. J. Goebel, Ann. Phys. (N.Y.) **104**, 145 (1977).
[16]A. Thiel, W. Greiner, and W. Scheid, Phys. Rev. C **29**, 864 (1984).
[17]J. Y. Park, W. Greiner, and W. Scheid, Phys. Rev. C **21**, 958 (1980).